Structure of Silicate Glasses and Melts at High Pressure: Quantum Chemical Calculations and Solid-State NMR

Sung Keun Lee*

Geophysical Laboratory, Carnegie Institution of Washington, 5251 Broad Branch Road, Washington, D.C. 20015

Received: November 24, 2003; In Final Form: February 10, 2004

Despite their strong implications for magmatic processes in the earth's interior and pressure-induced structural changes in other amorphous, covalent oxide materials, little is known, beyond the coordination numbers of the framework cations, about the structures of silicate melts and glasses at high pressure. Here, we use multinuclear (^{27}Al and ^{17}O) solid-state NMR and quantum chemical calculations to study the structures of silicate glasses quenched from melts at pressures up to 10 GPa in a multianvil apparatus. The pressure-induced changes in atomic configurations in the silicate melts include the formation of highly coordinated framework units such as $^{[5,6]}$Al and $^{[5,6]}$Si and bridging oxygens linking these framework units and the presence of nonbridging oxygens coordinated by network-modifying cations and $^{[5,6]}$Si. The proportion of high-pressure configurations such as $^{[5,6]}$Al−O−$^{[4]}$Si increases with pressure, but the fraction of nonbridging oxygen (Na−O−$^{[4]}$Si) decreases with pressure, leading to an increase of polymerization in melts. In bridging and nonbridging oxygens and highly coordinated framework units, structurally relevant NMR parameters (e.g., the isotropic chemical shift, δ_{iso}, and quadrupolar coupling product, P_q) show a pressure dependence. Quantum chemical calculations for model silicate clusters show that ^{17}O δ_{iso} for $^{[n]}$(Si,Al)−O−$^{[4]}$Si mainly increases with increasing coordination number *n*. Although ^{17}O δ_{iso} appears to be affected by longer-range interactions, it shows relatively moderate positive correlation with the $^{[n]}$(Si,Al)−O bond length and appears to decrease with the distance between Na and bridging oxygens. ^{17}O δ_{iso} for each oxygen cluster ($^{[n]}$(Si,Al)−O−$^{[4]}$Si) obtained from ^{17}O 3QMAS (triple quantum magic-angle spinning) NMR also increases with coordination number *n*. This is consistent with quantum calculations, implying that the $^{[n]}$(Si,Al)−O bond length may increase while the Na−O distance decreases with pressure. Although the overall variation ^{17}O P_q for each oxygen site is not significant, the ^{17}O P_q value of $^{[4]}$Si−O−$^{[4]}$Si seems to decrease with increasing pressure, suggesting that the $^{[4]}$Si−O−$^{[4]}$Si angle may decrease with densification. The ^{27}Al P_q for $^{[n]}$Al increases with increasing pressure, which implies that the distortion of the network unit increases with pressure. The widths of ^{17}O δ_{iso} distributions for $^{[n]}$(Si,Al)−O−$^{[4]}$Si increase with increasing pressure, which implies that bond lengths and angle distributions get wider with pressure. This trend is also consistent with the increasing distortion of framework polyhedra, suggested by increases in ^{27}Al P_q with pressure. The topological entropy was introduced to quantify the degree of randomness in the distributions of internal variables such as bond angle and length.

1. Introduction

Revealing the atomic structure of amorphous oxide has long been one of the fundamental unsolved problems in condensed matter physics, materials chemistry, glass science, and earth science. Silicate glasses and melts, in particular, have received tremendous attention because they are the key glass formers for diverse, technologically important amorphous materials and have essential implications for geochemical processes related to magma dynamics and properties.

To better understand the relationships between atomic structure and macroscopic properties for silicate glasses and melts with varying thermodynamic variables (e.g., temperature, pressure, and composition), it is necessary to know their atomic arrangements and the extent of chemical and topological disorder (in bond angle and length). It is well known that the covalent oxide glasses and melts, such as silicates and aluminosilicates, have rather well-defined coordination environments for framework cations (e.g., $^{[4]}$Al and $^{[4]}$Si) linked by bridging oxygen (BO, e.g., $^{[4]}$Al−O−$^{[4]}$Si). Adding network-modifying cations (e.g., K^+, Na^+, Ca^{2+}) leads to the formation of nonbridging oxygen (NBO, e.g., $^{[n]}$Na−O−$^{[4]}$Si). A number of macroscopic thermodynamic and transport properties of melts depend on the extent of polymerization (i.e., NBO fraction), which has often been assumed from chemical compositions of the glasses and melts at ambient pressure.[1]

Understanding the effect of pressure on the atomic configurations and the extent of disorder of the silicate glasses and melts can be of immense importance.[2] This would provide a mechanism for the densification of these materials under pressure and the changes in corresponding macroscopic properties. (See Wolf and McMillan[3] for a review.) Understanding the pressure effects would therefore elucidate the microscopic origins of anomalous macroscopic properties (e.g., decreasing viscosity with increasing pressure in silicate melts) and the corresponding geochemical processes in the earth's interior (e.g., generation, transport and emplacement of magma). Despite this importance, the pressure-induced structural changes in amorphous silicates at high pressure have not been well known beyond the

* E-mail: s.lee@gl.ciw.edu.

10.1021/jp037575d CCC: $27.50
Published on Web 04/17/2004

coordination number of framework cations or indirect information on topological changes. One reason for this is the small sample volume (typically a few milligrams of oxides) available in high-pressure experiments. Another reason is the inhomogeneous broadening of peaks (or modes) from conventional vibrational spectroscopy in diamond anvil cells, which is driven by inherent disorder in the glasses.[3] These difficulties often result in nonunique interpretations of local structures of high-pressure silicate melts. Furthermore, conventional scattering methods do not provide an explicit provision for the degree of intermixing among the framework units, which is known to control configurational thermodynamic properties such as configurational heat capacity, enthalpy, and the activity coefficient of oxides.[4−7]

Not suffering from these size constraints, experimental studies on glass and melt structures at ambient pressure have made rapid progress in recent years, allowing us to explore the distributions of cations and anions in amorphous materials. One of these notable advances includes a solid-state NMR technique that can yield information about element-specific atomic arrangements around nuclides of interest.[8] Particularly effective is ^{17}O NMR. Since the pioneering studies,[9−12] ^{17}O NMR has been applied to several crystalline silicates[11,13−15] and oxide glasses.[16−18] The advent and development of ^{17}O 3QMAS (triple quantum magic-angle spinning) NMR, which can greatly reduce the peak broadening due to residual second-order quadrupolar interactions,[19] yielded improved prospects for exploring atomic configurations around oxygen in diverse crystalline silicates including zeolites,[20−24] layer silicates,[25,26] chain silicates,[27] nesosilicates,[28] some organic solids,[29,30] and especially in various complex oxide glasses.[6,31−35] For instance, ^{17}O 3QMAS NMR of amorphous glasses has yielded structural details such as the connectivity among framework units and the degree of intermixing,[5,33,36] distributions of network-modifying cations in mixed-cation silicate glasses,[37−39] and topological disorder.[7,40]

These methodological advances can be applied to oxide glasses formed from high-pressure melts made with conventional equipment such as the multianvil apparatus. More recently, we used ^{17}O 3QMAS NMR to report the framework disorder and connectivity among highly coordinated framework units, such as $^{[5,6]}$Si in high-pressure silicate and aluminosilicate glasses quenched from melts at high pressure. These results show chemical ordering among these highly coordinated Si atoms at high pressure, favoring the formation of BOs that link $^{[4]}$Si and $^{[5,6]}$Si.[41]

The structurally relevant NMR parameters, including the isotropic chemical shift (δ_{iso}) and the quadrupolar coupling product (P_q) of quadrupolar nuclides (e.g., ^{27}Al and ^{17}O), are sensitive to variations in local symmetry and atomic configurations.[8,42] The pressure dependence of the NMR parameters of the oxygen species and framework units can provide important constraints on pressure-induced structural changes. It is thus essential to explore the NMR characteristics of those potential BOs (e.g., $^{[5,6]}$(Al, Si)−O−$^{[4]}$Si) and NBO sites prevalent at high pressure and in highly coordinated framework units. Systematic studies of ^{17}O NMR parameters have shown that the ^{17}O C_q (quadrupolar coupling constant) tends to increase with the Si−O−Si bond angle and slightly decreases with the Si−O bond length.[18,43,44] The ^{17}O C_q also depends on the number of charge-balancing cations around the BO as well as the metal−BO distance.[45] The isotropic chemical shift, a measure of the shielding of the magnetic field around nuclides by electrons, was shown to increase with the metal−BO distance[14,46] and the Si−O distance[27] for BO and NBO. As far as we know, NMR characteristics (parameters and their relationships to local structures) of silicate glasses at high pressure have not yet been systematically studied.

In this paper, we present ^{17}O and ^{27}Al MAS and 3QMAS (triple quantum magic-angle spinning) NMR spectra for silicate glasses in the system $[(Na_2O)_{1-x}(Al_2O_3)_x]3SiO_2$ (where $x = 0$, 0.25, and 0.5) quenched from liquids at high pressure in a multianvil apparatus. This system was chosen to explore the effect of polymerization on silicate melt structure at high pressure. The utility of the 3QMAS NMR with the site-population analyses in the study of silicate and aluminosilicate melt structures at high pressure was previously demonstrated.[41,47] Here, we primarily explore the detailed NMR characteristics of these new oxygen sites and framework cations at high pressure, using solid-state NMR and quantum chemical calculations, to better understand the relationship between NMR parameters and atomic configurations. Finally, we discuss the topological distribution in silicate glasses and introduce topological entropy to quantify how the distributions of internal variables vary in width and how their widths affect the transport and thermodynamic properties of melts.

2. Computational and Experimental Methods

2.1. Quantum Chemical Calculations. To gain insight into the relationship between the local configurations and NMR parameters for $^{[5,6]}$Si and $^{[5,6]}$Al and the possible oxygen sites linking these units at high pressure, quantum chemical calculations were performed with Gaussian 98[48,49] for model clusters that represent possible configurations in silicate glasses and melts at high pressure. Clusters containing $^{[6]}$Si and $^{[4]}$Si (i.e., $Na^{[6]}Si^{[4]}Si_4O_5(OH)_{12}$) as well as $^{[4,5,6]}$Al and $^{[4]}$Si (i.e., $NaSi_3^{[4]}AlO_4(OH)_8$, $Na^{[5]}Al^{[4]}Si_4O_5(OH)_{11}$, and $Na^{[6]}Al^{[4]}Si_4O_5(OH)_{12}$) were optimized at the Hatree−Fock (HF) level of theory with a 6-311G(d) basis set. The sodium in each model cluster considers the effect of sodium on the isotropic chemical shift as recently demonstrated in binary and ternary silicate glasses with varying types of network-modifying or charge-balancing cations.[6,38] The oxygen sites in these clusters include $^{[4]}$Si−O−T where T represents $^{[4,5,6]}$Si and $^{[4,5,6]}$Al. All oxygens except BOs are terminated with hydrogen for charge balance. There are no symmetry constraints except those involving the terminating hydrogen; the hydrogen−oxygen bond length and the angles containing hydrogen (H−O−Si) are identical for each framework unit. The clusters containing highly coordinated framework units were confined in four-membered rings such that as the coordination number for framework units increases, the distortion of the cluster may increase; this is because the $^{[n]}$Si(or Al)−O bond length increases with coordination number n. This confinement was introduced to simulate the effect of pressure. A $Na^{[6]}Al^{[4]}Si_4O_5(OH)_{12}$ cluster in a four-membered ring was not stable, and one of the $^{[6]}$Al−O bonds gets longer, eventually forming $^{[5]}$Al during the relaxation of the total energy. We thus chose a configuration with a fixed $^{[6]}$Al−O bond length of 2.206 Å, which satisfies Gaussian 98's convergence criteria for displacement (but not for force).

NMR chemical shielding tensors were calculated using the gauge-independent atomic orbital (GIAO) methods at the B3LYP/6-311+G(2d,p) level of theory for the above clusters.[48] The isotropic chemical shift for $^{[n]}$Si is calculated from the chemical shielding difference between an external reference (tetramethylsilane) and $^{[n]}$Si in the clusters. Isotropic chemical shielding for oxygen sites and Al sites is presented without calibration to standards. The results for $^{[5]}$Si ($Na^{[5]}Si^{[4]}Si_4O_5(OH)_{11}$) clusters were previously reported.[41] It should be noted

TABLE 1: Equilibrium Geometries and NMR Parameters of Oxygen [^{17}O Chemical Shielding (Up)] and Silicon Sites [^{29}Si Chemical Shielding (Bottom)] in Model Silicate Clusters Calculated from Quantum Chemical Calculations

oxygen cluster		Na−O (Å)	Si−O−Si (deg)	$^{[4]}$Si−O (Å)	$^{[4]}$Si−O (Å)	$^{[5,6]}$Si−O (Å)	ave $^{[4]}$Si−O (Å)[a]	chemical shielding (ppm)[a]
				$Na^{[6]}Si^{[4]}Si_4O_5(OH)_{12}$:$^{[6]}$Si Cluster				
O(1)	$^{[6]}$Si−O−$^{[4]}$Si	2.299	139.03	1.573		1.815	1.694	200.77
O(2)	$^{[6]}$Si−O−$^{[4]}$Si	2.213	129.89	1.590		1.831	1.710	199.73
O(3)	$^{[6]}$Si−O−$^{[4]}$Si	2.942	137.94	1.568		1.784	1.676	208.05
O(4)	$^{[4]}$Si−O−$^{[4]}$Si	4.000	146.80	1.615	1.624		1.619	234.34
O(5)	$^{[4]}$Si−O−$^{[4]}$Si	4.387	137.45	1.638	1.611		1.625	236.11
				$Na^{[5]}Si^{[4]}Si_4O_5(OH)_{11}$[b]: $^{[5]}$Si Cluster				
O(1)	$^{[5]}$Si−O−$^{[4]}$Si	3.065	136.65	1.593		1.668	1.631	217.09
O(2)	$^{[5]}$Si−O−$^{[4]}$Si	2.327	134.83	1.617		1.691	1.654	220.55
O(3)	$^{[5]}$Si−O−$^{[4]}$Si	2.531	139.035	1.585		1.753	1.669	207.03
O(4)	$^{[4]}$Si−O−$^{[4]}$Si	3.927	151.35	1.609	1.622		1.616	235.90
O(5)	$^{[4]}$Si−O−$^{[4]}$Si	4.348	151.72	1.615	1.618		1.616	234.43

Si cluster	chemical shielding (ppm)	chemical shift (ppm)
	$Na^{[6]}Si^{[4]}Si_4O_5(OH)_{12}$	
$^{[6]}$Si	521.34	−193.95
$^{[4]}$Si	407.33−421.70	(−79.94)−(−94.31)
	$Na^{[5]}Si^{[4]}Si_4O_5(OH)_{11}$	
$^{[5]}$Si	473.67	−146.28
$^{[4]}$Si	416.09−428.00	(−88.70)−(−100.61)
TMS[c]	327.39	

[a] NMR chemical shielding can be used to calculate the isotropic chemical shift from the difference between chemical shielding (C. S.) of the reference and the cluster: ^{17}O d_{iso} = C. S. (reference) − C. S. (BO sites). Here we report C. S. of the oxygen sites, which provides the isotropic chemical shift difference among the sites. Note that on the basis of the shielding scale of Wasylishen and Bryce, C. S. of the reference, H_2O(l) is 287.5 ± 0.6 ppm.[63] [b] The results (Na−O distance, bond angle, and chemical shielding) for $Na^{[5]}Si^{[4]}Si_4O_5(OH)_{11}$ were presented in Lee et al..[41] [($^{[4]}$Si−O) bond length + T′−O bond length]/2 in $^{[4]}$Si−O−T′ species (T′ are $^{[4]}$Si, $^{[5]}$Si, and $^{[6]}$Si). [c] Foresman and Frisch.[49]

that calculated NMR chemical shielding tensors depend on choice of basis sets, energy level of theory, and cluster size.[48,49]

2.2. Sample Preparation. Three sodium silicate and aluminosilicate glasses, $[(Na_2O)_{1-x}(Al_2O_3)_x]\cdot 3SiO_2$ (where $x = 0$, 0.25, and 0.5), were synthesized from Na_2CO_3, Al_2O_3, and 40% ^{17}O-enriched SiO_2. About 0.2 wt % cobalt oxide was added to enhance spin−lattice relaxation. Details of the sample synthesis are described elsewhere.[41,47] The glass starting materials were synthesized at 1 atm by fusing the mixtures for 1 h at 1473−1773 K in a He or Ar environment and were loaded into a multianvil apparatus with a $^{10}/_5$ and a $^{18}/_{11}$ (octahedron edge length/truncated edge length of the anvils) assembly.[50] The samples were fused at approximately 1923−2173 K for about 20 min and quenched to glasses over a pressure range of 6−10 GPa. The initial quench rate was estimated to be larger than 500 °C/s. The volumes of the samples from the $^{18}/_{11}$ and the $^{10}/_5$ assembly are typically about 7 and 2 mm^3, respectively.

2.3. NMR Spectroscopy. ^{17}O and ^{27}Al MAS and 3QMAS NMR spectra were collected on a CMX Infinity 300 spectrometer (7.1 T) at Larmor frequencies of 78.2 MHz for ^{27}Al and 40.7 MHz for ^{17}O, with a 2.5-mm ZrO_2 rotor in a Chemagnetic MAS probe. The recycle delay for ^{17}O and ^{27}Al MAS NMR was 1 s, with radio-frequency pulse lengths of 0.15 μs, which is about a 15° tip angle for the central transition in solids. ^{17}O and ^{27}Al 3QMAS NMR spectra were collected using a shifted-echo pulse sequence[8,42] composed of two hard pulses with durations of 3.3 and 0.75 μs and with the third soft pulse with a duration of 13 μs. Recycle delays for ^{17}O and ^{27}Al 3QMAS NMR vary from 1−3 s, depending on their spin−lattice relaxation time. The sample spinning speed was 19 kHz. The spectra were referenced to $AlCl_3$ for ^{27}Al and tap water for ^{17}O.

3. Results and Discussion

3.1. Quantum Chemical Calculations. *3.1.1. Equilibrium Geometry.* Tables 1 and 2 summarize the equilibrium geometries of the clusters and the corresponding isotropic chemical shielding of each oxygen species and framework unit, optimized from quantum chemical calculations. Figure 1 exhibits the optimized silicate and aluminosilicate clusters.

Sodium Silicate Clusters ($Na^{[6]}Si^{[4]}Si_4O_5(OH)_{12}$ and $Na^{[5]}Si^{[4]}Si_4O_5(OH)_{11}$). The average $^{[6]}$Si−O bond length in oxygen clusters is about 1.810 Å and is longer than those of $^{[4]}$Si−O (1.606 Å) and $^{[5]}$Si−O (1.704 Å). The $^{[4]}$Si−O bond length in $^{[6]}$Si−O−$^{[4]}$Si is about 1.568−1.590 Å and is shorter than that in $^{[4]}$Si−O−$^{[4]}$Si (1.611−1.638 Å). Similar trends can be seen in $^{[5]}$Si−O−$^{[4]}$Si sites (Table 1). The distribution of $^{[n]}$Si−O bond lengths for $^{[5,6]}$Si−O is somewhat wider than for $^{[4]}$Si−O in $^{[5,6]}$Si−O−$^{[4]}$Si sites. The increase in the Si−O distribution is also reflected in the ^{17}O 3QMAS NMR spectra of silicate glasses at high pressure, where the peak width for individual $^{[n]}$Si−O−$^{[4]}$Si peaks in the isotropic dimension increases with increasing pressure and the chemical shift dispersion of $^{[5,6]}$Si−O−$^{[4]}$Si is wider than that of $^{[4]}$Si−O−$^{[4]}$Si. (See the NMR result below.)

In crystalline silicates and aluminosilicates, it is known that the Si−O bond length is inversely correlated to the Si−O−Si bond angle.[51,52] Under the constraints of a four-membered ring, there is also a weak inverse correlation between bond angle and length from quantum chemical calculations (Table 1). The $^{[5,6]}$Si−O−$^{[4]}$Si angle is found to be smaller than the bond angle for $^{[4]}$Si−O−$^{[4]}$Si. Puckering of the ring increases with the increasing coordination of Si in four-membered rings, as indicated by the decrease in the average bond angle in the rings from 144.2° for the $^{[5]}$Si cluster to 138.0° for the $^{[6]}$Si cluster (Figure 1 and Table 1). Although there may be no strong correlation between the [Na−(Si−O−Si)] distance and the Si−O bond length in $^{[4]}$Si−O−$^{[n]}$Si on average, [Na−($^{[4]}$Si−O−$^{[6]}$Si)] is apparently shorter than [Na−($^{[4]}$Si−O−$^{[4]}$Si)].

Sodium Aluminosilicate Clusters ($NaSi_3^{[4]}AlO_4(OH)_8$, $Na^{[5]}Al^{[4]}Si_4O_5(OH)_{11}$, and $Na^{[6]}Al^{[4]}Si_4O_5(OH)_{12}$). As shown in Figure 1 and Table 2, the average $^{[n]}$Al−O bond length in $^{[n]}$Al−

TABLE 2: Equilibrium Geometries and NMR Parameters of Oxygen [^{17}O Chemical Shielding (Up)] and Aluminum Sites [^{27}Al Chemical Shielding (Bottom)] in Model Aluminosilicate Clusters Calculated from Quantum Chemical Calculations

oxygen cluster		Na−O (Å)	Si−O−Si or Si−O−Al (deg)	$^{[4]}$Si−O (Å)	$^{[4]}$Si−O (Å)	$^{[4,5,6]}$Al−O (Å)	ave Si(Al)−O (Å)[a]	chemical shielding (ppm)
			$Na^{[6]}Al^{[4]}Si_4O_5(OH)_{12}$:$^{[6]}$Al Cluster					
O(1)	$^{[6]}$Al−O−$^{[4]}$Si	2.252	133.10	1.569		1.928	1.748	220.01
O(2)	$^{[6]}$Al−O−$^{[4]}$Si	2.189	121.13	1.564		2.206	1.885	224.43
O(3)	$^{[6]}$Al−O−$^{[4]}$Si	2.376	141.02	1.553		1.943	1.748	227.84
O(4)	$^{[4]}$Si−O−$^{[4]}$Si	3.864	145.47	1.625	1.625		1.625	232.09
O(5)	$^{[4]}$Si−O−$^{[4]}$Si	4.442	138.58	1.665	1.602		1.633	233.40
			$Na^{[5]}Al^{[4]}Si_4O_5(OH)_{11}$:$^{[5]}$Al Cluster					
O(1)	$^{[5]}$Al−O−$^{[4]}$Si	3.065	134.11	1.573		1.825	1.699	236.75
O(2)	$^{[5]}$Al−O−$^{[4]}$Si	2.327	128.61	1.588		1.841	1.715	237.15
O(3)	$^{[5]}$Al−O−$^{[4]}$Si	2.531	139.39	1.562		1.897	1.729	229.26
O(4)	$^{[4]}$Si−O−$^{[4]}$Si	3.927	142.27	1.625	1.626		1.625	230.28
O(5)	$^{[4]}$Si−O−$^{[4]}$Si	4.348	139.76	1.611	1.644		1.628	233.14
			$NaSi_3{}^{[4]}AlO_4(OH)_8$:$^{[4]}$Al Cluster					
O(1)	$^{[4]}$Al−O−$^{[4]}$Si	4.048	152.39	1.570		1.733	1.651	262.69
O(2)	$^{[4]}$Al−O−$^{[4]}$Si	2.357	155.93	1.579		1.782	1.681	254.23
O(3)	$^{[4]}$Si−O−$^{[4]}$Si	4.760	138.08	1.616	1.634		1.625	232.19
O(4)	$^{[4]}$Si−O−$^{[4]}$Si	4.167	152.28	1.609	1.617		1.613	240.68

Al cluster	chemical shielding (ppm)
$Na^{[6]}Al^{[4]}Si_4O_5(OH)_{12}$	
$^{[6]}$Al	553.26
$^{[4]}$Si	399.92−419.50
$Na^{[5]}Al^{[4]}Si_4O_5(OH)_{11}$	
$^{[5]}$Al	529.01
$^{[4]}$Si	407.66−420.96
$NaSi_3{}^{[4]}AlO_4(OH)_8$	
$^{[4]}$Al	503.03
$^{[4]}$Si	425.51−428.24

[a] [($^{[4]}$Si−O) bond length + T′−O bond length]/2 in $^{[4]}$Si−O−T′ species (T′ are $^{[4]}$Si, $^{[4]}$Al, $^{[5]}$Al, and $^{[6]}$Al).

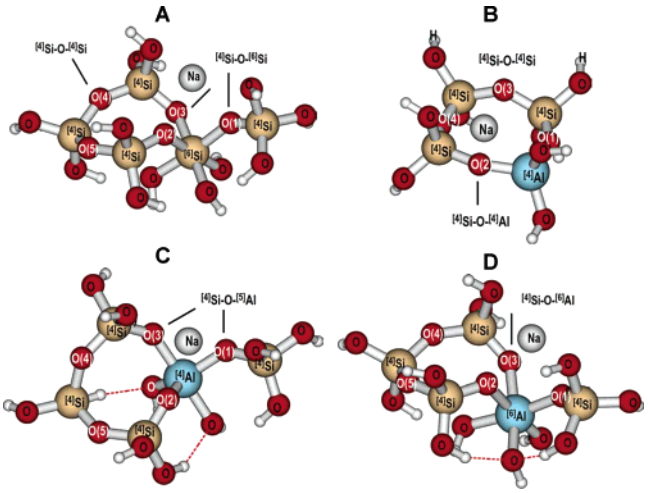

Figure 1. (A) Optimized geometries of bridging oxygen sites with $^{[6]}$Si. O(1), O(2), and O(3) are oxygen linking $^{[6]}$Si and $^{[4]}$Si ($^{[6]}$Si−O−$^{[4]}$Si). O(4) and O(5) are $^{[4]}$Si−O−$^{[4]}$Si. (B) Optimized geometry of aluminosilicate clusters with $^{[4]}$Al. O(1) and O(2) are $^{[4]}$Si−O−$^{[4]}$Al. (C) Aluminosilicate cluster with $^{[5]}$Al. O(1), O(2), and O(3) are $^{[4]}$Si−O−$^{[5]}$Al. (D) $^{[6]}$Al cluster with four-membered ring. O(1), O(2), and O(3) refer to $^{[4]}$Si−O−$^{[6]}$Al. Dotted lines refer to hydrogen bonds.

O−$^{[4]}$Si increases with increasing n from 1.757 ($n = 4$) to 1.855 ($n = 5$) to 2.025 Å ($n = 6$). As in sodium silicate clusters, the $^{[4]}$Si−O distance in $^{[n]}$Al−O−$^{[4]}$Si appears to be shorter than that in $^{[4]}$Si−O−$^{[4]}$Si in the aluminosilicate clusters. The bond angle for $^{[5,6]}$Al−O−$^{[4]}$Si is found to be usually smaller than that for $^{[4]}$Si−O−$^{[4]}$Si. There is also a weak correlation between the bond angle of $^{[4,5,6]}$Al−O−$^{[4]}$Si and the $^{[n]}$Al−O bond length. Puckering of the ring also apparently increases with increasing n as manifested in Figure 1 (B−D)

3.1.2. NMR Parameters. No simple correlation was found between the ^{17}O isotropic chemical shielding of Si−O−Si and the short-range configuration in coesite (SiO_2 polymorph),[18] implying that ^{17}O chemical shielding also depends on long-range interactions (including the second or third coordination sphere). However, previous studies reported that ^{17}O chemical shielding of Si−O−Si shows a negative correlation with the radii of alkali and alkaline earth metal cations and thus with the metal−oxygen distance.[14,46] It was also reported that chemical shielding for BO increases with decreasing Si−O bond length.[27] Note that the isotropic chemical shift increases with decreasing isotropic chemical shielding. Recent quantum calculations also reported a rather weak positive correlation between the Si−O−Si bond angle and ^{17}O isotropic chemical shielding for crystalline silicates.[53] Although it may be difficult to establish simple correlations between ^{17}O isotropic chemical shielding and the short-range structures, the inverse relationship between bond angle and length implies that ^{17}O isotropic chemical shielding may roughly decrease with the Si−O bond length. This trend is consistent with reports about other silicates.[27]

As shown in Table 1 and Figure 2A, ^{17}O isotropic chemical shielding of $^{[n]}$Si−O−$^{[4]}$Si decreases with increasing coordination number n and roughly increases with decreasing Si−O bond length in $^{[n]}$Si−O−$^{[4]}$Si. It also appears to be affected by the Na−O length and bond angle, though the correlation is not strong (Table 1). ^{17}O isotropic chemical shielding of $^{[n]}$Al−O−$^{[4]}$Si in aluminosilicate clusters decreases (isotropic chemical shift thus increases) with increasing coordination number n and shows negative correlation with the average $^{[n]}$(Al, Si)−O bond

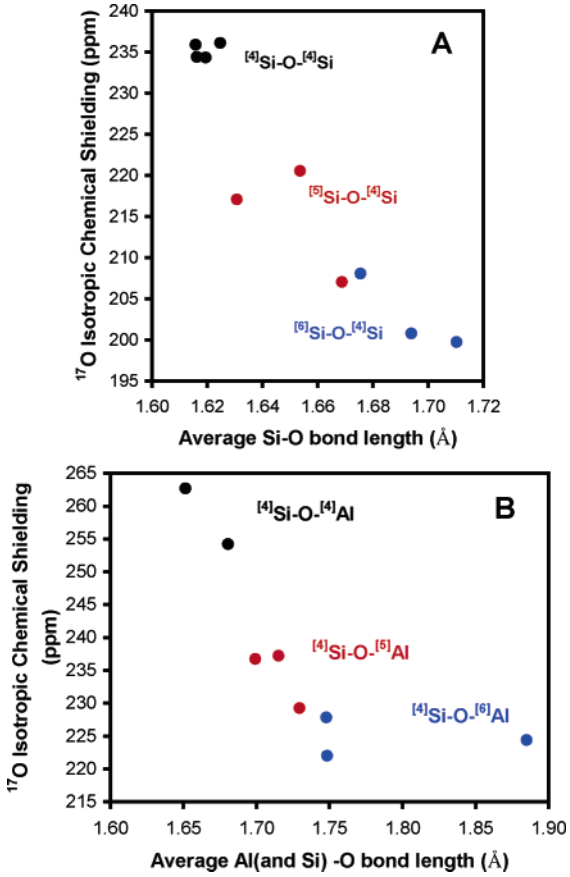

Figure 2. (A) Relationship between the average Si−O bond length and ^{17}O isotropic chemical shielding (ppm), calculated from quantum chemical calculations for the model clusters. Results for $^{[5]}$Si−O−$^{[4]}$Si are from Lee et al.[41] Blue, red, and black symbols show ^{17}O isotropic chemical shielding for $^{[6]}$Si−O−$^{[4]}$Si, $^{[5]}$Si−O−$^{[4]}$Si, and $^{[4]}$Si−O−$^{[4]}$Si, respectively. Note that with increasing chemical shielding, the isotropic chemical shift decreases. (B) Relationship between average Si(Al)−O bond length and isotropic chemical shielding for $^{[4]}$Si−O−$^{[4]}$Al (black symbols), $^{[4]}$Si−O−$^{[5]}$Al (red), and $^{[4]}$Si−O−$^{[6]}$Al (blue), respectively.

length in the oxygen clusters (Figure 2B and Table 2). O(2) in the $^{[6]}$Al cluster has a $^{[6]}$Al−O distance of 2.206 Å and a $^{[4]}$Si−O−$^{[6]}$Al angle of 121.13°(Figure 1D) and deviates from the linear relationship between the $^{[n]}$(Al, Si)−O bond length and isotropic chemical shielding, which may be due to the much smaller bond angle of this BO and suggests that ^{17}O chemical shielding may increase with increasing bond angle.

^{29}Si chemical shielding increases with the coordination number of Si. As shown in Table 1, the ^{29}Si chemical shift for $^{[4]}$Si varies from −80 to −100 ppm. Calculated ^{29}Si chemical shifts for $^{[5]}$Si and $^{[6]}$Si are about 50 and 100 ppm more shielded than that for $^{[4]}$Si, respectively, consistent with the experimental data for crystalline silicates.[54] $^{[4]}$Si appears to be more shielded (has a smaller isotropic chemical shift) in silicate clusters with $^{[5]}$Si than in the clusters with $^{[6]}$Si, suggesting that there is a systematic effect on the chemical shift of the next-nearest Si neighbors (e.g., $Q^4(m^{[n]}Si)$, where m is the number of $^{[n]}$Si next-nearest neighbors around $^{[4]}$Si) with respect to the chemical shift of Si. ^{29}Si chemical shielding for aluminosilicate glasses is also affected by the presence of $^{[n]}$Al as a next-nearest neighbor so that the chemical shielding for $^{[4]}$Si in these $^{[4]}$Al clusters is larger than that for $^{[5,6]}$Al clusters (Table 2). Calculated ^{27}Al chemical shieldings for $^{[4]}$Al, $^{[5]}$Al, and $^{[6]}$Al are 553.26, 529.00, and 502.03 ppm, respectively. This trend is consistent with the experimental data for crystalline aluminosilicates.[16]

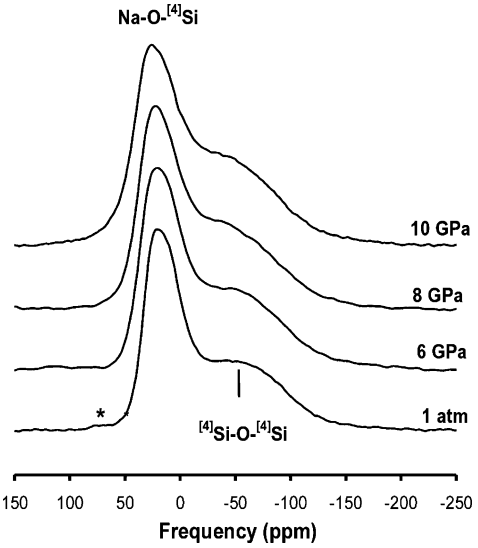

Figure 3. ^{17}O MAS NMR spectra for $Na_2O-3SiO_2$ glasses with varying pressure at 7.1 T. The asterisk (*) denotes the spinning sideband of the satellite transition. Glasses at 1 atm and 10 GPa were presented previously[41] and are shown here for comparison.

As shown in Tables 1 and 2 and in Figure 1, although the ^{17}O δ_{iso} collectively depends on the atomic configurations (including the T−O−T angle, length, and Na−O lengths or longer-range interactions), the trends given here are roughly consistent with those reported in previous work,[27] which shows that the isotropic chemical shift roughly increases with increasing (Si, Al)−O bond length and also appears to decrease with the Na−O distance.

3.2. NMR Results. *3.2.1. Sodium Trisilicate ($Na_2O{\cdot}3SiO_2$) Glasses (NS3).* Figure 3 shows ^{17}O MAS NMR spectra of NS3 quenched from melts at varying pressure where slight changes in peak shape and relative intensity between broad (BO) and narrow components (NBO, around 20 ppm) are clearly seen. The fraction of Na−NBO decreases with pressure, and the peak widths for both BO and NBO increase with pressure, as previously reported.[41]

Figure 4 shows ^{17}O 3QMAS NMR spectra with varying pressure for NS3, which clearly exhibits two types of BOs ($^{[4]}$Si−O−$^{[4]}$Si and $^{[4]}$Si−O−$^{[5,6]}$Si) and NBOs (Na−O−$^{[4]}$Si and Na−O−$^{[5,6]}$Si). The new peak at high pressure (around −80 ppm) in the isotropic dimension of 3QMAS NMR spectra was assigned to $^{[4]}$Si−O−$^{[5,6]}$Si on the basis of the above quantum chemical calculations (^{17}O isotropic chemical shielding difference) and the result from crystalline wadeite.[17,41] The fraction of this bridging oxygen cluster ($^{[4]}$Si−O−$^{[5,6]}$Si) increases with pressure. The peak around −40 ppm in the isotropic dimension may be due to the contribution from Na−O−$^{[5,6]}$Si.[41] The presence of considerable fractions of Na−O−$^{[5,6]}$Si at 6 GPa suggests that mainly NBOs (Na−O−$^{[4]}$Si) participate in compaction and that BOs do not seem to be involved at 6 GPa. The fractions of Na−O−$^{[4,5,6]}$Si and $^{[4]}$Si−O−$^{[4]}$Si further decrease above 6 GPa, suggesting that BO also participates in pressure-induced structural changes, forming $^{[4]}$Si−O−$^{[5,6]}$Si. The results for NS3 demonstrate the changes in coordination and connectivity with pressure in silicate glasses and melts, behavior that is not well manifested in ^{17}O MAS NMR spectra (Figure 3).

3.2.2. Sodium Aluminosilicate Glasses: $(Na_2O)_{0.75}(Al_2O_3)_{0.25}$-$3SiO_2$. (NAS150560) and $NaAlSi_3O_8$ Glasses (NAS6). Decreasing the number of network-modifying cations by replacing Na_2O with Al_2O_3 leads to increasing polymerization in silicates (i.e.,

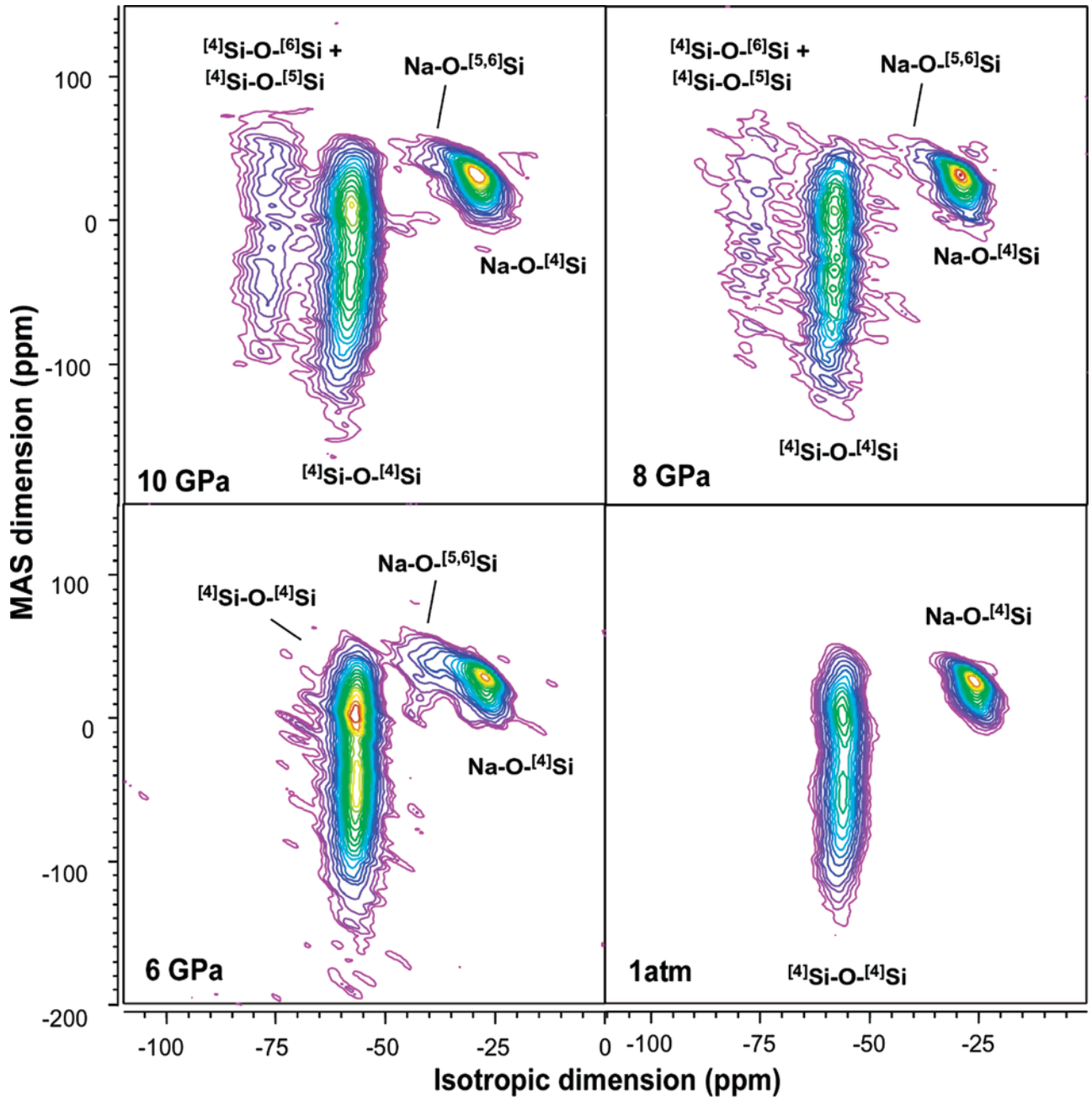

Figure 4. ^{17}O 3QMAS NMR spectra for $Na_2O-3SiO_2$ glasses quenched from melts at varying pressure as labeled. Contour lines are drawn at 5% intervals from 8 to 88% of the relative intensity, with added lines at the 4% and 6% levels to show low-intensity peaks better.

decreasing fractions of NBO). The coordination number of Al has been reported to increase with increasing pressure in depolymerized sodium aluminosilicate glasses.[55] Figure 5 shows the ^{27}Al MAS NMR spectra for sodium aluminosilicate glasses with varying degrees of polymerization and pressure. Whereas 7.1 T is relatively low field for ^{27}Al because of its large quadrupolar moment, the fractions of 4-, 5-, and 6-coordinated Al are each partially resolved. The longer tail on the lower-frequency shoulder suggests the distribution of quadrupolar coupling constants and isotropic chemical shifts in this glass, which is typical for covalent aluminosilicate glasses.[6] Whereas $^{[4]}Al$ is the dominant Al species at 1 atm, the fraction of highly coordinated Al increases with pressure.[55] Figure 6 presents isotropic projections of the ^{27}Al 3QMAS NMR spectra for NAS150560 with pressure. The improved resolution among different Al coordination sites demonstrates again that the fractions of $^{[5,6]}Al$ increase with pressure.

Figure 7 shows the ^{17}O MAS NMR spectra for NAS150560 and NAS6 glasses. The fraction of Na−NBO (narrow components around 20 ppm) appears to decrease, and the width of the NBO peak increases, which is behavior similar to that observed in NS3 (Figure 7 top).[41] The ^{17}O MAS NMR spectrum for NAS150560 at 8 GPa shows a small peak around 130 ppm (Figure 7, bottom), which might be related to Na−O−Al or other high-pressure configurations (e.g., 3-coordinated oxygen) not observed at 1 atm. Further studies at higher pressure should be necessary to confirm the assignment. Peak overlap among NBOs and BOs in MAS NMR spectra does not provide explicit information about framework connectivity in these glasses and melts.

Figure 8 shows ^{17}O 3QMAS NMR spectra for NAS150560, which yield much improved resolution for each NBO and BO site at high pressure. As pressure increases to 6 GPa, a new BO site, $^{[4]}Si-O-^{[5,6]}Al$, is observed (−45 ppm in the isotropic

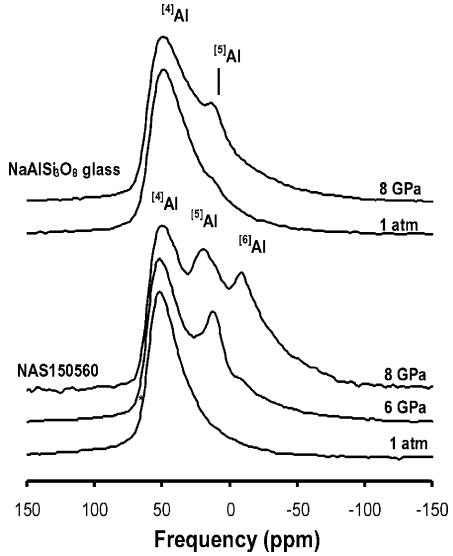

Figure 5. ^{27}Al MAS NMR spectra for $(Na_2O)_{0.75}(Al_2O_3)_{0.25}3SiO_2$ glasses and $NaAlSi_3O_8$ glasses with varying pressure at 7.1 T.

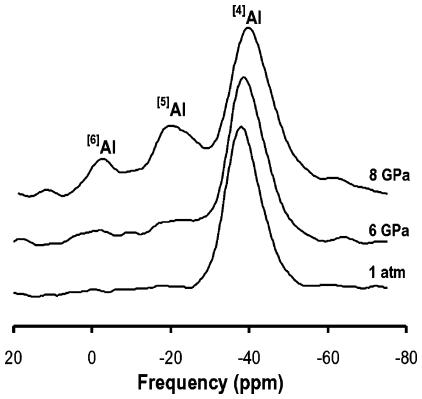

Figure 6. Isotropic projections of ^{27}Al 3QMAS NMR spectra for $(Na_2O)_{0.75}(Al_2O_3)_{0.25}3SiO_2$ glasses with varying pressure at 7.1 T.

dimension). This assignment is based on the above quantum chemical calculations and the presence of $^{[5,6]}$Al in these glasses. The fraction of $^{[4]}$Si−O−$^{[5,6]}$Al increases with pressure. As in the NS3, there is also a small fraction of Na−O−$^{[5,6]}$Si at 8 GPa. Although there are considerable fractions of $^{[4]}$Si−O−$^{[5,6]}$Si in NS3 at 8 GPa, only a negligible amount of this cluster (about −80 ppm) was observed in NAS150560 at 8 GPa, indicating that Al is more likely than Si to become highly coordinated at high pressure.[55,56]

NAS6 glasses are fully polymerized at 1 atm. Al and Si in NAS6 are predominantly 4-coordinated and connected by corner-sharing BOs ($^{[4]}$Si−O−$^{[4]}$Si and $^{[4]}$Si−O−$^{[4]}$Al). Figure 9 shows the ^{27}Al 3QMAS NMR spectra for NAS6 and NAS150560 glasses. Whereas there is evidence that $^{[5]}$Al is present in NAS6 at 8 GPa, the fraction of $^{[5]}$Al is much smaller than in NAS150560. This demonstrates that the fractions of these highly coordinated framework units depend on the presence of NBOs, which are deeply involved in mechanisms of pressure-induced structural changes. While topological rearrangement can be a favorable compaction mechanism for NAS6, the highly coordinated framework units are more likely to form for the NS3 and NAS150560 glasses, which have significant numbers of NBOs.

Figure 10 shows ^{17}O 3QMAS NMR spectra for NAS6 glasses with pressure. It is shown that the width of each peak in the isotropic dimension increases at 8 GPa. Note that the intensities

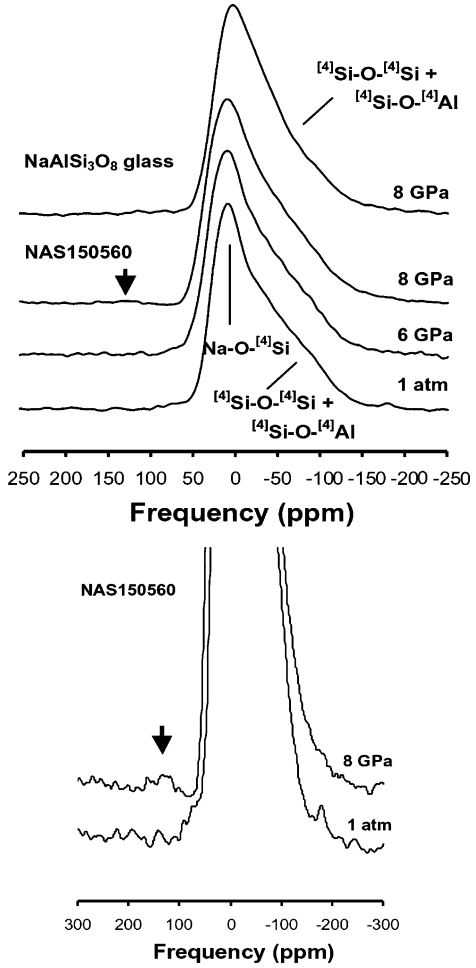

Figure 7. ^{17}O MAS NMR spectra for $(Na_2O)_{0.75}(Al_2O_3)_{0.25}3SiO_2$ glasses with varying pressure at 7.1 T. Arrow shows the peak that may be related to Al−NBO oxygen sites.

near −45 ppm in the isotropic dimension may suggest the presence of $^{[4]}$Si−O−$^{[5]}$Al, as indicated by the presence of $^{[5]}$Al in this glass (Figure 9).

3.2.3. NMR Parameters for High-Pressure BO, NBO, and Al Clusters. The variations with pressure of NMR parameters for the oxygen and framework cations can provide important constraints on changes in atomic configurations and topology with pressure. Table 3 summarizes the NMR parameters for oxygen sites in sodium silicate and aluminosilicate glasses with varying pressure. Here, NMR parameters were obtained from the center of gravity of each peak or peak positions (for the peaks with relatively low intensity and overlapped with other peaks, e.g., Na−O−$^{[5]}$Si) in both dimensions (e.g., see refs 6 and 42 for more information).

As shown in Table 3 and Figure 11, the ^{17}O isotropic chemical shift of $^{[n]}$(Si,Al)−O−$^{[4]}$Si generally increases with *n*. As shown from quantum chemical calculations (Figure 2) and as reported previously for crystalline chain silicates,[27] the isotropic chemical shift may increase with the Si−O bond length. This trend can certainly explain the isotropic chemical shift difference among $^{[n]}$(Si,Al)−O−$^{[4]}$Si species with increasing coordination number. (With increasing *n*, the Si−O or Al−O bond length increases, and thus the isotropic chemical shift increases.) The isotropic chemical shift of each oxygen cluster, $^{[n]}$(Si,Al)−O−$^{[4]}$Si, also increases with increasing pressure, suggesting that Si−O and Al−O bond lengths in both NBOs (Na−O−$^{[4]}$Si) and BOs may increase with increasing pressure. This trend may also be related to the decrease in the Na−O distance with pressure, as

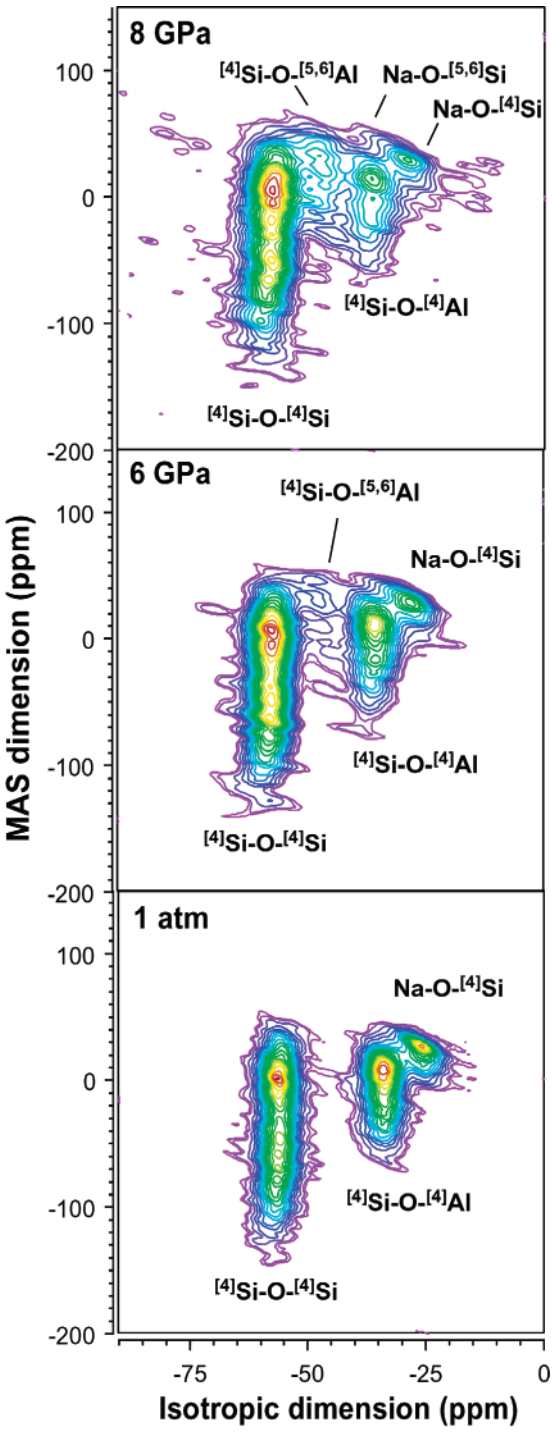

Figure 8. ^{17}O 3QMAS NMR spectra for $(Na_2O)_{0.75}(Al_2O_3)_{0.25}3SiO_2$ glasses with varying pressure at 7.1 T. Contour lines are drawn at 5% increments from 8 to 98% of the relative intensity, with added lines at 6% to show low-intensity peaks better.

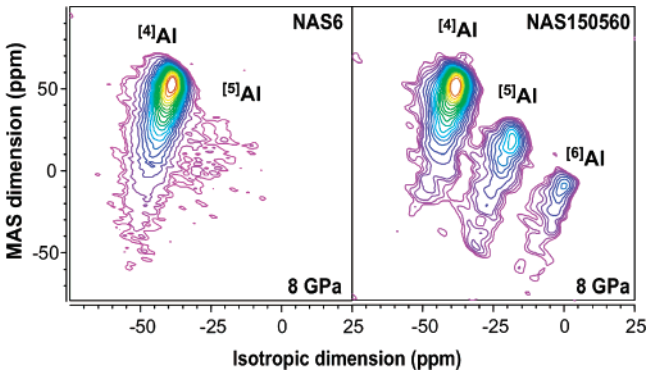

Figure 9. ^{27}Al 3QMAS NMR spectra for $NaAlSi_3O_8$ and $(Na_2O)_{0.75}(Al_2O_3)_{0.25}3SiO_2$ glasses at 8 GPa and 7.1 T.

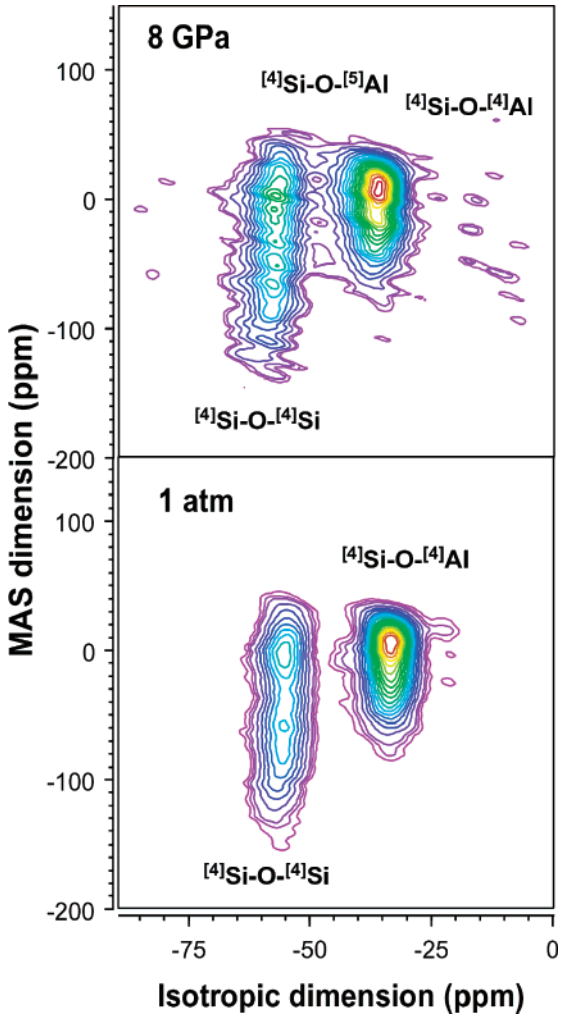

Figure 10. ^{17}O 3QMAS NMR spectra for $NaAlSi_3O_8$ glasses with varying pressure at 7.1 T. Contour lines are drawn at 5% increments from 8 to 88% of the relative intensity, with added lines at the 4% and 6% levels to show low-intensity peaks better.

mentioned above. It should be noted that the small increase in ^{17}O δ_{iso} for $^{[5,6]}Si-O-^{[4]}Si$ can also be due to the increasing contribution of $^{[6]}Si-O-^{[4]}Si$ with pressure. The bond length of each oxygen cluster can increase in these systems, in part by reducing the bond angle and possibly by increasing the population of smaller rings.

Figure 12 illustrates the variation of the ^{17}O quadrupolar coupling product, P_q, with pressure. (Here, $P_q = C_q\,(1 + \eta^2/3)^{1/2}$, where $0 \le \eta \le 1$ is the quadrupolar asymmetry parameter.) For the glasses studied here (NAS6, NAS150560, and NS3), the ^{17}O P_q of $^{[4]}Si-O-^{[4]}Si$ slightly decreases with increasing pressure. For NAS6, the ^{17}O P_q for $^{[4]}Si-O-^{[4]}Si$ decreases from 4.96 (1 atm) to 4.85 MHz (8 GPa), and the ^{17}O P_q for NS3 varies from 4.85 MHz (1 atm) to 4.73 MHz (8 GPa). Previous studies have shown that the ^{17}O P_q increases with increasing bond angle.[18,43−45,57] Here, we note that the variation of P_q with pressure is not prominent (Figure 12) and that changes in the $^{[4]}Si-O-^{[4]}Si$ bond angle from 140 to 130° lead to only about a 0.3 MHz decrease in calculated P_q.[45] Notwithstanding, the observed trend may suggest that the average $^{[4]}Si-O-^{[4]}Si$ angle decreases with pressure. Values for $^{[5,6]}Si-O-^{[4]}Si$ are larger

TABLE 3: NMR Parameters (^{17}O δ_{iso} and P_q) of Oxygen Sites in Sodium Silicate and Aluminosilicate Glasses with Varying Pressure[a]

	O site	δ_{iso} (ppm)	P_q (MHz)	populations (%)[c]
	$Na_2O-3SiO_2$ glass (NS3)			
1 atm	Na−O−[4]Si	38.1 (±1)	2.1 (±0.1)	28.0 (±1.5)
	[4]Si−O−[4]Si	52.3 (±1)	4.9 (±0.1)	72.0 (±1.5)
6 GPa	Na−O−[4]Si	41.2 (±2)	2.2 (±0.2)	18.1 (±2)
	Na−O−[5,6]Si[b]	58.8 (±2)	2.3 (±0.2)	7.5 (±2)
	[4]Si−O−[4]Si	55.0 (±1)	4.8 (±0.2)	70.0 (±2)
	[4]Si−O−[5,6]Si[b]			4.9 (±2)
8 GPa	Na−O−[4]Si	42.4 (±2)	2.2 (±0.2)	22.4 (±2)
	Na−O−[5,6]Si[b]	58.8 (±2)	2.3 (±0.2)	2.7 (±2)
	[4]Si−O−[4]Si	58.1 (±1)	4.7 (±0.1)	61.5 (±2)
	[4]Si−O−[5,6]Si	81.9 (±2)	5.2 (±0.2)	13.4 (±1.5)
10 GPa	Na−O−[4]Si	43.1 (±1)	2.2 (±0.1)	18.9 (±1.5)
	Na−O−[5,6]Si[b]	56.9 (±2)	1.7 (±0.2)	3.2 (±2)
	[4]Si−O−[4]Si	58.2 (±1)	4.7 (±0.1)	22.7 (±1.5)
	[4]Si−O−[5,6]Si	82.7 (±1)	5.2 (±0.1)	55.2 (±1.5)
	$NaAlSi_3O_8$ glass (NAS6)			
1 atm	[4]Si−O−[4]Al	35.1 (±1)	3.5 (±0.1)	50 (±1.5)
	[4]Si−O−[4]Si	47.8 (±1)	5.0 (±0.1)	50 (±1.5)
8 GPa	[4]Si−O−[4]Al	39.6 (±3)	3.6 (±0.2)	48 (±2.5)
	[4]Si−O−[4]Si	54.7 (±1)	4.9 (±0.1)	52 (±1.5)
	$(Na_2O)_{0.75}(Al_2O_3)_{0.25}3SiO_2$ glass (NAS150560)			
1 atm	Na−O−[4]Si	35.7 (±1)	2.2 (±0.1)	12.1 (±1.5)
	[4]Si−O−[4]Al	36.4 (±1)	3.4 (±0.1)	30.4 (±1.5)
	[4]Si−O−[4]Si	52.0 (±1)	4.9 (±0.1)	57.5 (±1.5)
6 GPa	Na−O−[4]Si	41.8 (±1)	2.0 (±0.2)	8.2 (±2)
	Na−O−[5,6]Si[b]	54.2 (±2)	1.7 (±0.3)	<1
	[4]Si−O−[4]Al	38.9 (±1)	3.4 (±0.2)	27.0 (±2)
	[4]Si−O−[5,6]Al[b]	58.9 (±3)	3.5 (±0.2)	5.4 (±2)
	[4]Si−O−[4]Si	56.2 (±1)	4.8 (±0.2)	59.4 (±2)
8 GPa	Na−O−[4]Si	43.5 (±1)	1.9 (±0.1)	7.4 (±1.5)
	Na−O−[5,6]Si[b]	56.1 (±3)	2.0 (±0.25)	1.2
	[4]Si−O−[4]Al	42.1 (±1)	3.5 (±0.1)	17.0 (±1.5)
	[4]Si−O−[5,6]Al[b]	59.9 (±3)	3.6 (±0.2)	12.2 (±2)
	[4]Si−O−[4]Si	57.4 (±1)	4.8 (±0.1)	58.4 (±1.5)
	[4]Si−O−[5,6]Si	85.6 (±2)	5.0 (±0.2)	3.9 (±2)

[a] Numbers in parentheses refer to uncertainty of the NMR parameters and populations. [b] NMR parameters were obtained from the peak positions. [c] Calibrated population considering MQMAS efficiency with the magnitude of quadrupolar interactions and experimental conditions.[6,64]

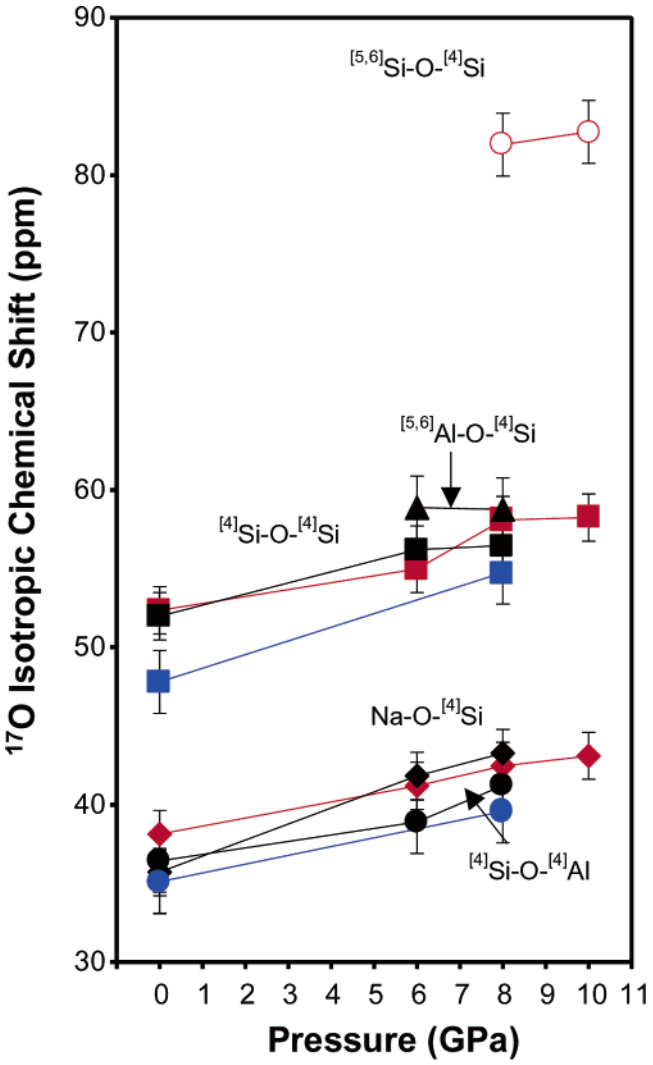

Figure 11. Variation of ^{17}O δ_{iso} of oxygen sites in sodium silicate and aluminosilicate glasses with pressure. Closed circles, diamonds, squares, and triangles refer to [4]Al−O−[4]Si, Na−O−[4]Si, [4]Si−O−[4]Si, and [5,6]Al−O−[4]Si, respectively. Open circles and diamonds denote [5,6]Si−O−[4]Si and Na−O−[5,6]Si, respectively. Red, blue, and black symbols show oxygen sites in NS3, NAS6, and NAS150560 glasses, respectively.

(about 5.2 MHz) than those for [4]Si−O−[4]Si. Although the correlation between the ^{17}O P_q of Si−O−Al (or [5,6]Si−O−[4]Si) and the bond angle has not been established, these values for [4]Si−O−[4]Al vary little with pressure, and ^{17}O P_q for [5,6]Al−O−[4]Si apparently increases with pressure (Table 3). The P_q of Na−O−[4]Si in NS3 slightly increases with pressure, but that in NAS150560 shows the opposite pressure dependence. This may imply a difference in Na coordination around NBOs with varying degrees of polymerization.

Figure 13 shows the variation of the ^{27}Al P_q of [n]Al with pressure. The ^{27}Al P_q of [n]Al increases with increasing pressure, demonstrating that the local distortion of the electric-field gradient increases with pressure, and thus the distribution of bond angle and length around Al may be more variable with pressure. The ^{27}Al isotropic chemical shift for [n]Al does not vary much with pressure (Table 4). The ^{27}Al δ_{iso} values of [4]Al, [5]Al, and [6]Al are about 61.5, 26.5, and −2.0 ppm, respectively, consistent with previous experimental results[16,58] and quantum chemical calculations (Table 2). In turn, the distortion due to the increasing variation in the Al−O bond length at Al sites causes the oxygen isotropic chemical shifts to vary with pressure, consistent with ^{17}O NMR results where the width of each peak increases with pressure. (See below for further discussion.) The width of the [4]Al peak in the isotropic projection of ^{27}Al 3QMAS NMR spectra for NAS150560 shows little variation (peak position and width) with pressure, suggesting that pronounced P_q increases with pressure mainly stem from increases in average P_q with pressure (Figure 6).

Figure 14 shows the variation of peak widths for oxygen sites in the isotropic dimension for ^{17}O 3QMAS NMR spectra; the peak widths increase with pressure. The average ^{17}O δ_{iso} also increases with pressure, mostly because bond lengths increase or bond angles decreases. There is a larger distribution of these internal variables (bond angle and length) at higher pressure, implying an increase in the topological contribution to total configurational entropy.[40]

3.3. Extent of Disorder and Macroscopic Properties of Melts at High Pressure. The experimental results given above clearly show that atomic configurations (cation and anion environments) in silicate glasses and melts at high pressure are significantly different from those at 1 atm. These pressure-induced structural changes include the formation of highly

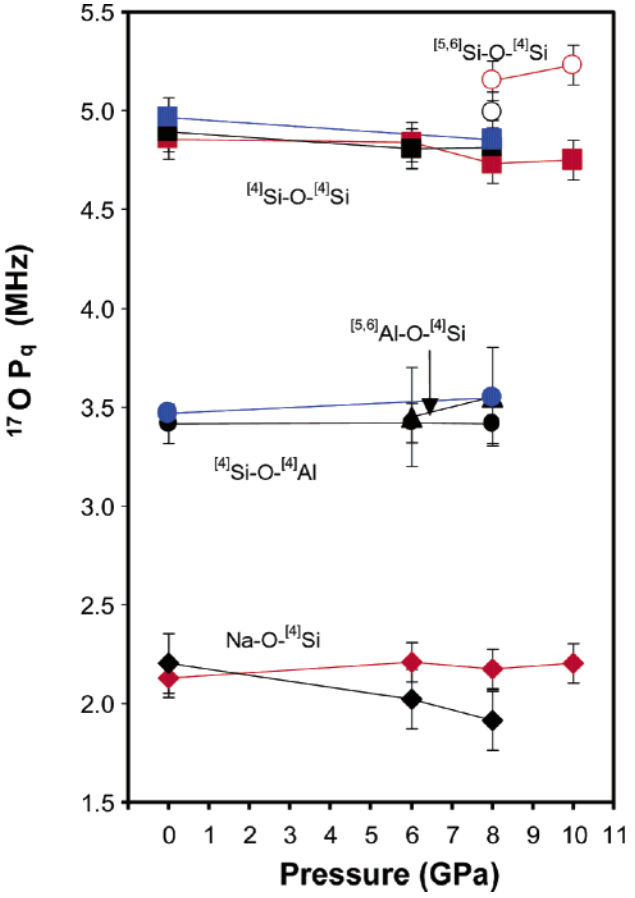

Figure 12. Variation of ^{17}O P_q of oxygen species in sodium silicate and aluminosilicate glasses with pressure. Closed circles, diamonds, squares, and triangles refer to [4]Al−O−[4]Si, Na−O−[4]Si, [4]Si−O−[4]Si, and [5,6]Al−O−[4]Si, respectively. Open circles denote [5,6]Si−O−[4]Si. Red, blue, and black symbols show oxygen sites in NS3, NAS6, and NAS150560 glasses, respectively.

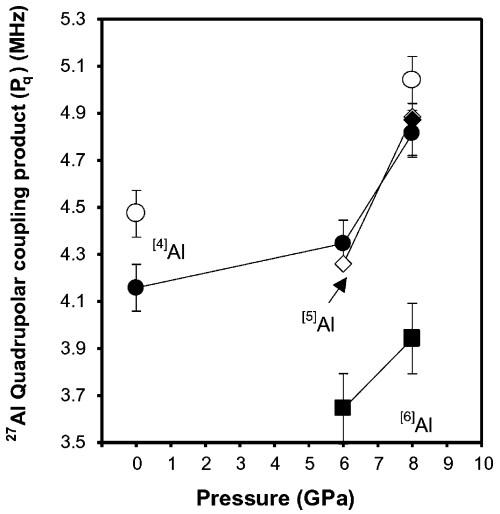

Figure 13. Variation of NMR quadrupolar coupling product (P_q) of the Al site with pressure. The uncertainty of P_q was included. Circles, diamonds, and squares refer to P_q values of [4]Al, [5]Al, and [6]Al, respectively. Open and closed symbols denote P_q values of Al sites in $NaAlSi_3O_8$ glasses and NAS150560 glasses, respectively. The thick solid line shows the trend for P_q of [4]Al in NAS150560 glass.

coordinated framework units and thus the formation of both BOs linking these units and NBOs coordinated by network-modifying cations and highly coordinated frameworks. The distribution of these units certainly deviates from a random

TABLE 4: NMR Parameters (^{27}Al δ_{iso} and P_q) of Al Sites in Sodium Silicate and Aluminosilicate Glasses with Varying Pressure

	Al site	δ_{iso} (ppm)	P_q (MHz)	populations (%)[a]
		$NaAlSi_3O_8$ glass (NAS6)		
1 atm	[4]Al	62.3 (±3)	4.5 (±0.1)	100
8 GPa	[4]Al	61.9 (±3)	5.0 (±0.1)	91.8 (±2)
	[5]Al	33.5 (±3)	4.9 (±0.25)	8.2 (±2.5)
		$(Na_2O)_{0.75}(Al_2O_3)_{0.25}3SiO_2$ glass (NAS150560)		
1 atm	[4]Al	61.1 (±3)	4.2 (±0.1)	100
6 GPa	[4]Al	61.3 (±3)	4.3 (±0.1)	83.7 (±2)
	[5]Al	26.2 (±3)	4.3 (±0.1)	13.4 (±2)
	[6]Al	−2.2 (±3)	3.6 (±0.15)	2.9 (±2.5)
8 GPa	[4]Al	61.4 (±3)	4.8 (±0.1)	63.1 (±2)
	[5]Al	27.1 (±3)	4.9 (±0.1)	26.2 (±2)
	[6]Al	−1.8 (±3)	3.9 (±0.15)	10.7 (±2.5)

[a] Calibrated population considering MQMAS efficiency with the magnitude of quadrupolar interactions and experimental conditions.[6,64]

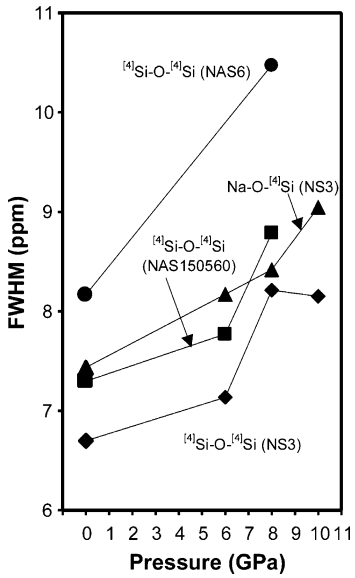

Figure 14. Variation of the fwhm of the oxygen peak in the isotropic projection of 3QMAS NMR spectra with pressure. Circles, squares, and diamonds denote [4]Si−O−[4]Si in NAS6, NAS150560, and NS3, respectively. Triangles refer to Na−O−[4]Si in NS3.

distribution such that the formation of Na−O−[4,5,6]Al, Al−O−Al, and [6]Si−O−[6]Al appears to be largely prohibited. Recent numerical simulations of the distribution of framework cations for the NS3 glass at 10 GPa[41] clearly indicate chemical ordering among the framework units, disfavoring clustering among the units.

Another inherent aspect of disorder is topological disorder due to bond-angle and bond-length distributions, which certainly contributes to the total configurational entropy of silicate glasses.[4] Bond angles for some BOs including [4]Si−O−[4]Si are likely to decrease with pressure, and the [n](Si, Al)−O length increases with pressure. Although it is difficult to quantify the topological entropy directly,[40] some aspects of it due to the bond-angle or bond-length distribution may be captured by the introduction of the following expression:

$$\Delta S = k \ln\left(\frac{\sigma_1}{\sigma_2}\right) \quad (1)$$

where ΔS is the topological entropy difference between states

1 and 2 and k is the Boltzman constant. σ_1 and σ_2 refer to the widths (either the fwhm or the standard deviation in the case of a normal distribution) of internal variables for states 1 and 2. Considering the rough linear correlation between the $^{[n]}$Si-(Al)−O bond length and ^{17}O δ_{iso}, the fwhm data in the isotropic dimension, presented in Figure 14, can be correlated with the T−O bond-length distribution. Note that to be rigorous we should extract the isotropic chemical shift from the chemical shift distribution in the 2D NMR spectra and convert it to a bond-length distribution.[40,59] As an approximation, here we use the fwhm for Si−O−Si in Figure 14 to examine the topological variation with pressure in silicate glasses as a function of polymerization and Si/Al. For NAS6, as pressure increases from 1 atm to 8 GPa, topological entropy increases by about 2.1 kJ/mol because of the distribution of Si−O; the same pressure increase causes 1.5 and 1.6 kJ/mol increases in NAS150560 and NS3, respectively. These results manifest the presence of pressure-induced topological entropy and also show that NAS6 is likely to undergo more severe topological variation with pressure. This is largely because of a lack of NBOs in NAS6, making topological variation the major mechanism for compaction.

Chemical ordering among framework units and the above topological entropy can contribute to total configurational entropy and other transport and configurational thermodynamic properties. From Adam−Gibbs theory[60,61] and Stokes−Einstein relations,[62] the following relations can be deduced:

$$\left(\frac{\partial \eta}{\partial P}\right)_T \propto -\left(\frac{\partial D(O^{2-})}{\partial P}\right)_T \propto -\left(\frac{\partial S_{config}}{\partial P}\right)_T \qquad (2)$$

where η is viscosity and $D(O^{2-})$ is the O^{2-} diffusivity in silicate melts. S_{config} is the total configurational entropy of silicate melts and may consist of a chemical contribution from framework disorder and a topological contribution. The variation of configurational entropy with pressure can be inferred from the microscopic analysis of the chemical ordering of framework units, along with the topological entropy from a wider distribution of internal variables, as shown here. Therefore, the microscopic information given here can provide atomistic constraints on the pressure dependence of viscosity or diffusivity, parameters that are relevant to magmatic processes. We also recently showed that the fraction of NBO in the system and its pressure dependence ($\partial X_{NBO}/\partial P$) can account for the anomalous behavior in transport properties of silicate melts with pressure;[47] for example, the O^{2-}diffusivity of partially polymerized sodium aluminosilicate melts increases with pressure and then decreases.[2] Because the detailed fraction of NBO and the glass structures as a function of pressure can be obtained as shown here, the detailed macroscopic properties with pressure can be inferred from the structure and the extent of disorder in the silicate glasses and melts. The methods (a combination of high-pressure equipment and 3QMAS NMR, together with quantum chemical calculations) and the results given here thus offer a new opportunity to study structures of other covalent oxide glasses and melts at high pressure, yielding microscopic origins of the macroscopic properties of oxide melts.

Acknowledgment. This research is supported by a Carnegie Postdoctoral Fellowship. I thank an anonymous reviewer for helpful and constructive comments. I appreciate the helpful discussions, support, and consideration of Drs. B. Mysen, G. D. Cody, and Y. Fei at the Geophysical Laboratory, and I thank Professor P. Grandinetti at The Ohio State University for RMN software. I also thank Drs. Z. Xu, S. Wang, and P. Zhao and Professor J. F. Stebbins from whom I learned 3QMAS NMR and pulse sequence coding during my 5 years of residence at Stanford University.

References and Notes

(1) Mysen, B. O. *Structure and Properties of Silicate Melts*; Elsevier: Amsterdam, 1988.
(2) Poe, B. T.; McMillan, P. F.; Rubie, D. C.; Chakraborty, S.; Yarger, J. L.; Diefenbacher, J. *Science* **1997**, *276*, 1245.
(3) Wolf, G. H.; McMillan, P. F. Pressure Effects on Silicate Melt Structure and Properties. In *Structure, Dynamics, and Properties of Silicate Melts*; Stebbins, J. F., McMillan, P. F., Dingwell, D. B., Eds.; Mineralogical Society of America: Washington, DC, 1995; Vol. 32, p 505.
(4) Lee, S. K.; Stebbins, J. F. *Am. Mineral.* **1999**, *84*, 937.
(5) Lee, S. K.; Stebbins, J. F. *Geochim. Cosmochim. Acta* **2002**, *66*, 303.
(6) Lee, S. K.; Stebbins, J. F. *J. Phys. Chem. B* **2000**, *104*, 4091.
(7) Lee, S. K.; Musgrave, C. B.; Zhao, P.; Stebbins, J. F. *J. Phys. Chem. B* **2001**, *105*, 12583.
(8) Engelhardt, G.; Michel, D. *High-Resolution Solid-State NMR of Silicates and Zeolites*; Wiley: New York, 1987.
(9) Geissberger, A. E.; Bray, P. J. *J. Non-Cryst. Solids* **1983**, *54*, 121.
(10) Schramm, S.; Kirkpatrick, R. J.; Oldfield, E. *J. Am. Chem. Soc.* **1983**, *105*, 2483.
(11) Timken, H. K. C.; Janes, N.; Turner, G. L.; Lambert, S. L.; Welsh, L. B.; Oldfield, E. *J. Am. Chem. Soc.* **1986**, *108*, 7236.
(12) Jellison, G. E.; Panek, L. W.; Bray, P. J.; Rouse, G. B. *J. Chem. Phys.* **1977**, *66*, 802.
(13) Walter, T. H.; Turner, G. L.; Oldfield, E. *J. Magn. Reson.* **1988**, *76*, 106.
(14) Timken, H. K. C.; Schramm, S. E.; Kirkpatrick, R. J.; Oldfield, E. *J. Phys. Chem.* **1987**, *91*, 1054.
(15) Mueller, K. T.; Wu, Y.; Chmelka, B. F.; Stebbins, J.; Pines, A. *J. Am. Chem. Soc.* **1990**, *113*, 32.
(16) Kirkpatrick, R. J. MAS NMR Spectroscopy of Minerals and Glasses. In *Spectroscopic Methods in Mineralogy and Geology*; Hawthorne, F. C., Ed.; Mineralogical Society of America: Washington, DC, 1988; p 341.
(17) Xue, X.; Stebbins, J. F.; Kanzaki, M. *Am. Mineral.* **1994**, *79*, 31.
(18) Grandinetti, P. J.; Baltisberger, J. H.; Farnan, I.; Stebbins, J. F.; Werner, U.; Pines, A. *J. Phys. Chem.* **1995**, *99*, 12341.
(19) Frydman, I.; Harwood, J. S. *J. Am. Chem. Soc.* **1995**, *117*, 5367.
(20) Loeser, T.; Freude, D.; Mabande, G. T. P.; Schwieger, W. *Chem. Phys. Lett.* **2003**, *370*, 32.
(21) Zhao, P.; Neuhoff, P. S.; Stebbins, J. F. *Chem. Phys. Lett.* **2001**, *344*, 325.
(22) Xu, Z.; Stebbins, J. F. *Solid State NMR* **1998**, *11*, 243.
(23) Bull, L. M.; Bussemer, B.; Anupold, T.; Reinhold: A.; Samoson, A.; Sauer, J.; Cheetham, A. K.; Dupree, R. *J. Am. Chem. Soc.* **2000**, *122*, 4948.
(24) Amoureux, J.-P.; Bauer, F.; Ernst, H.; Fernandez, C.; Freude, D.; Michel, D.; Pingel, U.-T. *Chem. Phys. Lett.* **1998**, *285*.
(25) Lee, S. K.; Stebbins, J. F.; Weiss, C. W.; Kirkpatrick, R. J. *Chem. Mater.* **2003**, *15*, 2605.
(26) Lee, S. K.; Stebbins, J. F. *Am. Mineral.* **2003**, *88*, 493.
(27) Ashbrook, S. E.; Berry, A. J.; Wimperis, S. *J. Phys. Chem. B* **2002**, *106*, 773.
(28) Ashbrook, S. E.; Berry, A. J.; Wimperis, S. *Am. Mineral.* **1999**, *84*, 1191.
(29) Wu, G.; Dong, S. *J. Am. Chem. Soc.* **2001**, *123*, 9119.
(30) Wu, G.; Dong, S.; Ida, R.; Reen, N. *J. Am. Chem. Soc.* **2002**, *124*, 1768.
(31) Wang, S.; Stebbins, J. F. *J. Non-Cryst. Solids* **1998**, *231*, 286.
(32) Wang, S.; Stebbins, J. F. *J. Am. Ceram. Soc.* **1999**, *82*, 1519.
(33) Dirken, P. J.; Kohn, S. C.; Smith, M. E.; Vaneck, E. R. H. *Chem. Phys. Lett.* **1997**, *266*, 568.
(34) Xu, Z.; Maekawa, H.; Oglesby, J. V.; Stebbins, J. F. *J. Am. Chem. Soc.* **1998**, *120*, 9894.
(35) Stebbins, J. F.; Xu, Z. *Nature* **1997**, *390*, 60.
(36) Lee, S. K.; Stebbins, J. F. *J. Non-Cryst. Solids.* **2000**, *270*, 260.
(37) Stebbins, J. F.; Oglesby, J. V.; Xu, Z. *Am. Mineral.* **1997**, *82*, 1116.
(38) Lee, S. K.; Stebbins, J. F. *J. Phys. Chem. B* **2003**, *107*, 3141.
(39) Lee, S. K.; Mysen, B. O.; Cody, G. D. *Phys. Rev. B* **2003**, *68*, 214206.
(40) Lee, S. K.; Stebbins, J. F. *Geochim. Cosmochim. Acta* **2003**, *67*, 1699.
(41) Lee, S. K.; Fei, Y.; Cody, G. D.; Mysen, B. O. *Gephys. Res. Lett.* **2003**, *30*, 1845.
(42) Baltisberger, J. H.; Xu, Z.; Stebbins, J. F.; Wang, S.; Pines, A. *J. Am. Chem. Soc.* **1996**, *118*, 7209.
(43) Clark, T. M.; Grandinetti, P. J. *J. Phys.: Condens. Matter* **2003**, *15*, s2387.

(44) Tossell, J. A.; Lazzeretti, P. *Phys. Chem. Mineral.* **1988**, *15*, 564.
(45) Vermillion, K. E.; Florian, P.; Grandinetti, P. J. *J. Chem. Phys.* **1998**, *108*, 7274.
(46) Clark, T. M.; Grandinetti, J. *J. Phys. Chem. B* **2001**, *105*, 12257.
(47) Lee, S. K.; Cody, G. D.; Fei, Y.; Mysen, B. O. *Geochim. Cosmochim. Acta*, in press, 2004.
(48) Frisch, M. J.; Trucks, G. W.; Schlegel, H. B.; Scuseria, G. E.; Robb, M. A.; Cheeseman, J. R.; Zakrzewski, V. G.; Montgomery, J. A., Jr.; Stratmann, R. E.; Burant, J. C.; Dapprich, S.; Millam, J. M.; Daniels, A. D.; Kudin, K. N.; Strain, M. C.; Farkas, O.; Tomasi, J.; Barone, V.; Cossi, M.; Cammi, R.; Mennucci, B.; Pomelli, C.; Adamo, C.; Clifford, S.; Ochterski, J.; Petersson, G. A.; Ayala, P. Y.; Cui, Q.; Morokuma, K.; Malick, D. K.; Rabuck, A. D.; Raghavachari, K.; Foresman, J. B.; Cioslowski, J.; Ortiz, J. V.; Stefanov, B. B.; Liu, G.; Liashenko, A.; Piskorz, P.; Komaromi, I.; Gomperts, R.; Martin, R. L.; Fox, D. J.; Keith, T.; Al-Laham, M. A.; Peng, C. Y.; Nanayakkara, A.; Gonzalez, C.; Challacombe, M.; Gill, P. M. W.; Johnson, B. G.; Chen, W.; Wong, M. W.; Andres, J. L.; Head-Gordon, M.; Replogle, E. S.; Pople, J. A. *Gaussian 98*, revision A.11; Gaussian, Inc.: Pittsburgh, PA, 1998.
(49) Foresman, J. B.; Frisch, A. *Exploring Chemistry with Electronic Structure Methods*, 2nd ed.; Gaussian Inc.: Pittsburgh, PA, 1996.
(50) Bertka, C. M.; Fei, Y. *J. Geophys. Res.* **1997**, *102*, 5251.
(51) Brown, G. E.; Gibbs, G. V.; Ribbe, P. H. *Am. Mineral.* **1969**, *54*, 1044.
(52) Gibbs, G. V. *Am. Mineral.* **1982**, *67*, 421.
(53) Profeta, M.; Mauri, E.; Pickard, C. J. *J. Am. Ceram. Soc.* **2003**, *125*, 541.
(54) Stebbins, J. F.; Poe, B. *Geophy. Res. Lett.* **1999**, *26*, 2521.
(55) Yarger, J. L.; Smith, K. H.; Nieman, R. A.; Diefenbacher, J.; Wolf, G. H.; Poe, B. T.; McMillan, P. F. *Science* **1995**, *270*, 1964.
(56) Waff, H. S. *Geophy. Res. Lett.* **1975**, *2*, 193.
(57) Clark, T. M.; Grandinetti, J. *Solid State NMR* **2000**, *16*, 55.
(58) Skibsted, J.; Henderson, E.; Jakobsen, H. J. *Inorg. Chem.* **1993**, *32*, 1013.
(59) Farnan, I.; Grandinetti, P. J.; Baltisberger, J. H.; Stebbins, J. F.; Werner, U.; Eastman, M.; Pines, A. *Nature* **1992**, *358*, 31.
(60) Adam, G.; Gibbs, J. H. *J. Chem. Phys.* **1965**, *43*, 139.
(61) Richet, P. *Geochim. Cosmochim. Acta* **1984**, *48*, 471.
(62) Shimizu, N.; Kushiro, I. *Geochim. Cosmochim. Acta* **1984**, *48*, 1295.
(63) Wasylishen, R. E.; Bryce, D. L. *J. Chem. Phys.* **2002**, *117*, 10061.
(64) Bak, M.; Rasmussen, J. T.; Nielsen, N. C. *J. Magn. Reson.* **2000**, *147*, 296.